Graphical abstract

Novel g-C_3N_4 quantum dots/$BiPO_4$ nanocrystals heterostructured photocatalysts have been synthesized; the photocatalytic activity for degradation of Methyl Orange as been significantly improved under visible light (λ>420 nm) irradiation.

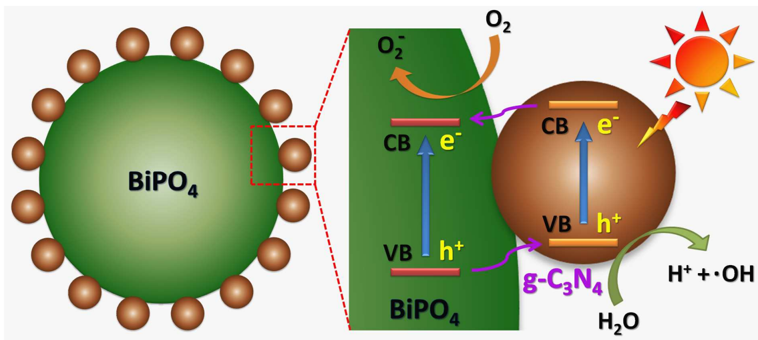

Journal Name RSCPublishing

COMMUNICATION

Novel visible light-induced g-C_3N_4 quantum dots/$BiPO_4$ nanocrystals composite photocatalysts for efficient degradation of methyl orange

11Cite this: DOI: 10.1039/x0xx00000x

Received 00th January 2012,
Accepted 00th January 2012

DOI: 10.1039/x0xx00000x

www.rsc.org/

Zesheng Li,*[a] Bolin Li,[a] Shaohong Peng,[a] Dehao Li, [a] Shiyan Yang, [b] Yueping Fang*[b]

[a] *Development Center of Technology for Petrochemical Pollution Control and Cleaner Production of Guangdong Universitites, College of Chemical Engineering, Guangdong university of Petrochemical Technology, Maoming, Guangdong, 525000, China;*
[b] *Institute of Biomaterial, College of Science, South China Agricultural University, Guangzhou, 510642, China.*
Corresponence author: Zesheng Li E-mail: lzs212@163.com; Yueping Fang E-mail: ypfang@scau.edu.cn.

Novel composite architectures made up of graphitic carbon nitride quantum dots/bismuth phosphate nanocrystals have been synthesized as a visible light-induced photocatalyst for efficient degradation of methyl orange.

The development of photocatalysts with high catalytic activity and good stability under sunlight is a key issue in photocatalysis science, and is also important in solving present environment and energy problems.[1] The creation of efficient photocatalysts utilizing visible light (~43% of the solar irradiance) instead of UV light (~4% of the solar irradiance) seems great significant for practical application.[2] Recently, there has been a great deal of research focused on the synthesis of quantum dots (QDs)-based composite semiconductor architectures, such as carbon QDs/Ag_3PO_4,[3] carbon QDs/Cu_2O,[4] CdS QDs/carbon nitride[5] and CdS QDs/graphene,[6] due to their outstanding dimensional effects, interfacial properties as well as multipurpose functionalities. As a result, the design of QDs-based composite is effective strategy to enhance the catalytic efficiency of photocatalysts under visible light irradiation.

Graphitic carbon nitride (g-C_3N_4) was found to be a stable and effective photocatalysts under solar light irradiation due to their remarkable electronic properties.[7] The catalytic applications of g-C_3N_4 include degradation of organic dyes, NO decomposition, Friedel-Crafts reactions, CO_2 reduction, and water splitting, etc.[8] Recently, many works presented that g-C_3N_4 as one commonly available and promising photocatalyst with visible light response has particular superiority for environment application.[9] However, there are still some limitations in the bulk g-C_3N_4 photocatalytic system, such as its low specific surface area and poor quantum yield.[10] Generally, several approaches including dimension reduction[11] and heterostructures[12] can be used to deal with these problems, because the nanostructures can endow with maximum specific surface area of active component, and the heterostructures can effectively decrease the recombination of photo-generated electrons and holes,[13] thus increasing the quantum efficiency of catalytic system. However, most of the reported g-C_3N_4 nanostructures are composed of stacked 2-D nanosheets,[14] and very few available examples concentrated on 0-D quantum dots exis,[15] especially on QD-based heterostructures.

Bismuth phosphate ($BiPO_4$), as a new type of oxy-acid salt photocatalyst, has proved to be of more superior photocatalytic activity than that of TiO_2 (P25) photocatalyst for the degradation of organic dye.[16] It is found that both the wider band gap (3.85 eV) and higher separation efficiency of electron-hole pairs contributed to the high photocatalytic activity of $BiPO_4$ photocatalyst.[17] Expressly, the inductive effect of PO_4^{3-} helps the e^-/h^+ separation, which plays an important role in its excellent photocatalytic activity.[16] Up to now, the most of previous applications of $BiPO_4$-based photocatalysts were limited to UV light.[18] To obtain a more efficient utilization of sunlight therefore, it is of great significance to develop efficient visible light (λ>420 nm) induced photocatalysts for organic dye photo-degradation.

In this communication, we demonstrate the creation of novel g-C_3N_4 quantum dots/$BiPO_4$ nanocrystals (g-C_3N_4 QDs/$BiPO_4$ NCs) composite architectures with significantly enhanced photocatalytic activity for degradation of Methyl Orange (MO) under visible light irradiation. For this composite system, three features have become apparent in previous reports: (i) unique g-C_3N_4 QDs in size of ~ 5 nm are successfully synthesized; (ii) spherical $BiPO_4$ NCs in diameter of ~60 nm are also achieved and (iii) novel heterostructures on the base of g-C_3N_4 QDs and $BiPO_4$ NCs are firstly created by a facile synthesis procedure. With these merits, we investigated that the MO photo-degradation with excellent performances, including high activity and stability, could be designed on the basis of such composite architectures.

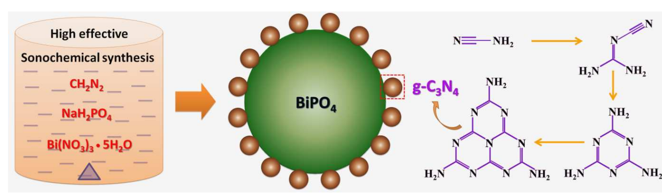

Fig. 1 Schematic processes for the formation of g-C_3N_4 QDs/$BiPO_4$ NCs composite by associated sonochemical and heat-treating synthesis.

For the synthesis (see ESI for details) of g-C_3N_4 QDs/$BiPO_4$ NCs composite architectures, a associated sonochemical and heat-treating synthesis was introduced, by using CH_2N_2, NaH_2PO_4 and $Bi(NO_3)_3$•$5H_2O$ as precursor materials. The integrated synthesis process of g-C_3N_4 QDs/$BiPO_4$ NCs composite and synthetic mechanism of g-C_3N_4 are schematically shown in Fig. 1. Firstly, the precursor ions of Bi^{3+} could be easily combined with PO_4^- to form deposited $BiPO_4$ NCs.[17] Meanwhile, the CH_2N_2 precursor can be evenly adsorbed on to the surface of $BiPO_4$ NCs under ultrasonic dispersion. Afterward, g-C_3N_4 QDs were formed and assembled on the surface of $BiPO_4$ NCs via a bottom-up growth from CH_2N_2 precursor,[7(a)] at the elevated temperature in subsequent procedure. Generally, the condensation pathway from Amino Cyanide to Dicyandiamide and later to Melamine and Melem was seen as a receivable synthetic mechanism to generate the slightly defect polymeric species of carbon nitride.[8(a)] It is noteworthy that all these NCs growth and QDs assemble processes can be accomplished by the facile sonochemical synthesis and heat-treatment procedure.

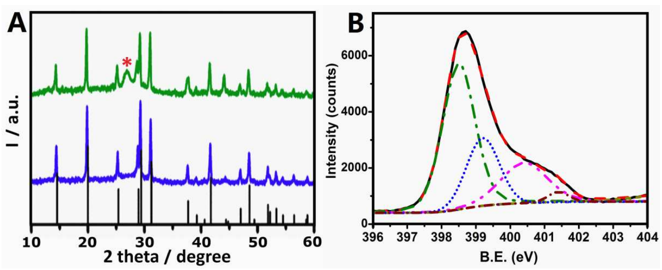

Fig. 2 (A) XRD patterns of g-C_3N_4 QDs/$BiPO_4$ NCs (green) and single $BiPO_4$ NCs (blue); (B) XPS spectrum (N 1s) of g-C_3N_4 QDs/$BiPO_4$ NCs.

In order to confirm the crystalline and atomic structures of the as-prepared g-C_3N_4 QDs/$BiPO_4$ NCs composite, the XRD and XPS analysis were carried out, respectively. Fig. 2 (A) shows the XRD patterns of g-C_3N_4 QDs/$BiPO_4$ NCs (green) and single $BiPO_4$ NCs (blue). Evidently, for the both samples, the same diffraction peaks of $BiPO_4$ (JCPDS 15-0766) have been detected, in which the peaks at $2\theta \approx 14.6^{o}$, 20.1^{o}, 25.5^{o}, 29.5^{o}, 31.3^{o}, 41.9^{o} and 48.7^{o} are corresponding to the diffraction peaks of (100), (101), (110), (200), (102), (211) and (212) crystal planes of $BiPO_4$.[16] The XRD pattern of g-C_3N_4 QDs/$BiPO_4$ NCs composite have an additional peak at $2\theta \approx 27.5^{o}$ (as labelled by *), corresponding to the inter-planar distance of d=0.324 nm, can be indexed as the (002) peak of the stacking of the conjugated aromatic system in g-C_3N_4.[7(a)] Fig. 2 (B) reveals the N 1s spectrum of g-C_3N_4 QDs/$BiPO_4$ NCs from XPS analysis. In this N 1s spectrum several binding energies can be separated, where the main signal peaks at 398.7 eV and 400.7 eV can be assigned to sp^2-hybridized nitrogen (C=N-C) groups and tertiary nitrogen (N-$(C)_3$) groups of g-C_3N_4, respectively.[7(a)] As a whole, the XRD and XPS results demonstrated that composite structures based on $BiPO_4$ and g-C_3N_4 phase have been successfully obtained by the present synthetic strategy.

The morphologies and structures of the samples in the present synthesis were further investigated by means of TEM technique, with the results shown in Fig. 3. Fig. 3 (A) and (B) display the typical TEM images of the single $BiPO_4$ NCs in different magnification, which indicate that the sample has an approximate spherical nanostructures. The diameter of $BiPO_4$ NCs ranges from 40 nm to 80 nm, and the dominant diameter would be about 60 nm (see Fig. 4 (A)). On the other hand, the detailed microstructures of g-C_3N_4 QDs/$BiPO_4$ NCs have been demonstrated in Fig. 3 (C) and (D). Obviously, multitudinous g-C_3N_4 QDs have been synthesized and uniformly distributed on the surface of $BiPO_4$ NCs. The diameter of g-C_3N_4 QDs ranges from 3 nm to 7 nm, and the dominant diameter would be about 5 nm (see Fig. 4 (B)). Remarkably, despite that the size of g-C_3N_4 QDs is very small, no secondary particle aggregation can be observed on the surface of $BiPO_4$ NCs, suggesting a good compatibility of the heterogeneous components of $BiPO_4$ and g-C_3N_4. For comparison, the single g-C_3N_4 sample was also achieved at the absence of bismuth nitrate while keeping other conditions unchanged in the synthesis. The TEM image and XRD pattern of the single g-C_3N_4 sample are shown in Fig. S1 (A) and (B), respectively. The results demonstrate that the single g-C_3N_4 sample has the same crystallographic structure (with a characteristic peak at $2\theta \approx 27.5^{o}$) as compared with g-C_3N_4 QDs, whereas the morphological structure of the single g-C_3N_4 sample is entirely different (with a porous fibre structure in size of 100 nm). It could be deduced that the $BiPO_4$ solid surface might play an important role in the formation of smaller g-C_3N_4 QDs, and the further studies toward the detailed growth mechanism are now underway. On the whole, it would be a promising innovation for the present study, as far as the quantum dot architecture concerned, relative to the previously reported g-C_3N_4 2-D nanostructures.

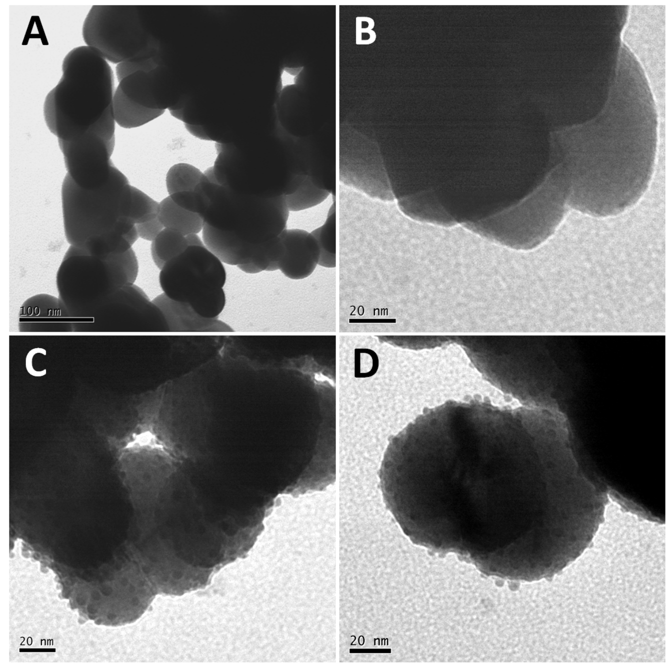

Fig. 3 Typical TEM images of the as-prepared samples: (A, B) single $BiPO_4$ NCs and (C, D) g-C_3N_4 QDs/$BiPO_4$ NCs.

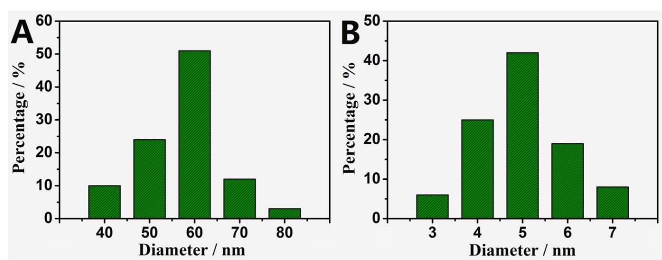

Fig. 4 Histograms of diameter distribution for (A) $BiPO_4$ NCs and (B) g-C_3N_4 QDs by TEM measurement.

As one important factor that may influence the photocatalytic properties, the BET specific surface area has been determined through the nitrogen adsorption/desorption measurements. The BET specific surface area of the single $BiPO_4$ NCs, g-C_3N_4 QDs/$BiPO_4$ NCs and single g-C_3N_4 samples is 8.3, 39.4 and 62.8, $m^2\ g^{-1}$, respectively. The higher surface area of single g-C_3N_4 sample should be derived from the lower density than the single $BiPO_4$ NCs sample. In addition, the mass content of $BiPO_4$ in the g-C_3N_4 QDs/$BiPO_4$ NCs is estimated to be 87.4 wt. % by the ICP analysis. Based on the mass content of g-C_3N_4 (namely 12.6 wt. %), it can be calculated that the potential specific surface area of g-C_3N_4 QDs is as high as 255 $m^2\ g^{-1}$, in which the specific surface area is beneficial for building photocatalysts with high activity.[10]

The visible light-induced photocatalytic activities of the as-prepared samples were evaluated by degradation of methylene orange (MO), a hazardous dye as well as a representative model to test the photodegradation capability of nanoarchitectures.[1(a)] Fig. 5

shows the photocatalytic activities and kinetics of the as-prepared photocatalysts including the single $BiPO_4$ NCs, single g-C_3N_4 and g-C_3N_4 QDs/$BiPO_4$ NCs (based on the composite) samples, for the degradation of MO dye in aqueous solution under visible-light irradiation. Obviously, the g-C_3N_4 QDs/$BiPO_4$ NCs composite photocatalyst exhibits a higher photocatalytic activity than the single g-C_3N_4 photocatalyst, where the MO can be decolored with about 92 % in 180 min for g-C_3N_4 QDs/$BiPO_4$ NCs, while the decolorization rate of single g-C_3N_4 was only about 75% (see Fig. 5 A). The first-order reaction rate constant can be calculated by the plots of the ln (C/C_0) v.s. radiation time (t). The obtained rate law may be ln (C/C_0) = $-kt$, where C is the concentration of dye, C_0 the initial concentration of dye, k the reaction rate constant, and t the irradiation time. The degradation rate constant k of g-C_3N_4 QDs/$BiPO_4$ NCs was estimated to be 0.0135 min^{-1}, which was 1.7 time as high as that of single g-C_3N_4 (0.0079 min^{-1}) (see Fig. 5 B). A contrast degradation experiment over single $BiPO_4$ NCs was also achieved, and the result showed that single $BiPO_4$ there is no obvious photocatalytic activity under visible-light irradiation, which is similar to the case without the use of catalyst.

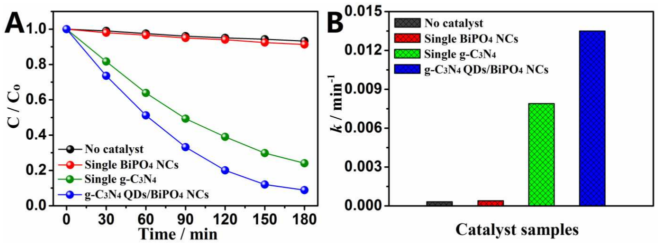

Fig. 5 Photocatalytic activities (A) and corresponding rate constant k (B) of MO degradation for the as-prepared photocatalysts.

In an attempt to learn about the potential activity of g-C_3N_4 component in the g-C_3N_4 QDs/$BiPO_4$ NCs composite, the photocatalytic activity was normalized on the base of component mass (see Fig. 6 A). Remarkably, the photocatalytic activity on the base of g-C_3N_4 QDs in g-C_3N_4 QDs/$BiPO_4$ NCs under visible irradiation can be estimated to be 13.5 times as high as that of single g-C_3N_4 sample. Understandably, the high activity of g-C_3N_4 QDs manly originates from the high specific surface area of g-C_3N_4 QDs[15] and the potential promoted effect from $BiPO_4$ NCs[16]. Furthermore, the photocatalitic activity was further normalized on the S_{BET} of g-C_3N_4 component, from which one can conclude the promoted effect of $BiPO_4$ component (see Fig. 6 B). Fortunately, the S_{BET} normalized photocatalytic activity was still 3.3 times that of single g-C_3N_4 sample, which clearly demonstrates that introducing $BiPO_4$ into g-C_3N_4 photocatalyst system can effectively enhance their photocatalytic activity.

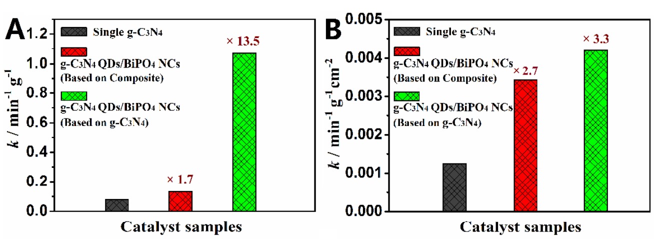

Fig. 6 Normalized photocatalytic activity based on the mass (A) and S_{BET} (B) of the designated component.

The stability of photocatalysts is another important issue for their assessment and application. Therefore, the cycling runs for the degradation of MO on the single g-C_3N_4 and g-C_3N_4 QDs/$BiPO_4$ NCs samples were further performed to evaluate the photocatalytic stability (see Fig. 7). After every 180 min of photodegradation, the photocatalysts were separated and washed with deionized water. The stability testing results illustrated that both the degradation rates of the two samples showed slightly decrease after the continuous four-run repeated irradiation within 720 min. The above mentioned results demonstrate that the obtained g-C_3N_4 QDs/$BiPO_4$ NCs composite can be used as a promising photocatalyst with excellent activity and desirable stability, for the degradation of MO in aqueous solution under visible irradiation.

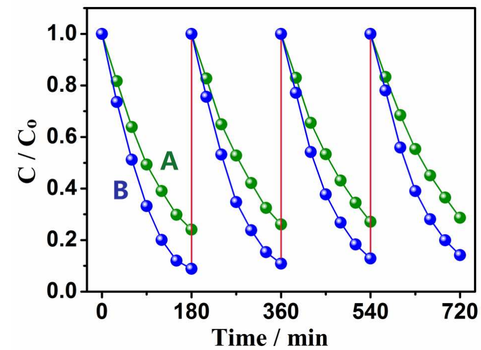

Fig.7 Cycling runs of MO degradation on (A) single g-C_3N_4 and (B) g-C_3N_4 QDs/$BiPO_4$ NCs photocatalyst.

The photocatalytic testing has shown excellent performances of the novel g-C_3N_4 QDs/$BiPO_4$ NCs composite. A possible mechanism for MO degradation on the g-C_3N_4 QDs/$BiPO_4$ heterostructured photocatalyst under visible light irradiation is proposed (see Fig. 8). Based on the band gap positions, the conduction band (CB) and valence band (VB) edge potentials of polymeric g-C_3N_4 were determined at −1.13 and +1.57 eV[18(b)], respectively. The CB and VB edge potentials of $BiPO_4$ were at –0.65 and +3.20 eV[18(b)], respectively. Because the CB and VB edge potentials of g-C_3N_4 were more negative than those of $BiPO_4$, the difference edge potentials allowed the electron transfer from the CB of g-C_3N_4 to that of $BiPO_4$. Meanwhile, the photogenerated holes on $BiPO_4$ can directly transfer to g-C_3N_4, making charge separation more efficient and the probability of photo-generated electron-hole recombination was reduced, resulting in enhanced photocatalytic activity and stabilization.

For a possible degradation process, the electrons on the $BiPO_4$ may capture the adsorbed O_2 on the composite catalyst surface and reduce it to $•O_2^-$. The hydrogen ions ionized from water molecular might be combined with the moderate $•O_2^-$ to form H_2O_2 molecular. H_2O_2 can then be further activated to the most reactive •OH by accepting a third photo-generated electron and cause the formation of •OH groups. On the other hand, the holes on the g-C_3N_4 can also bond with water to generate more •OH groups. Under the action of substantial strong oxidizing species, the structure of MO was destroyed and finally decomposed into degradation products. All these processes could be described as follows[19]:

$$e^- + O_2 \rightarrow •O_2^- \quad (1)$$

$$•O_2^- + e^- + 2H^+ \rightarrow H_2O_2 \quad (2)$$

$$H_2O_2 + e^- \rightarrow •OH + OH^- \quad (3)$$

$$h^+ + H_2O \rightarrow •OH + H^+ \quad (4)$$

$$•OH + MO \rightarrow \text{degradation products} \quad (5)$$

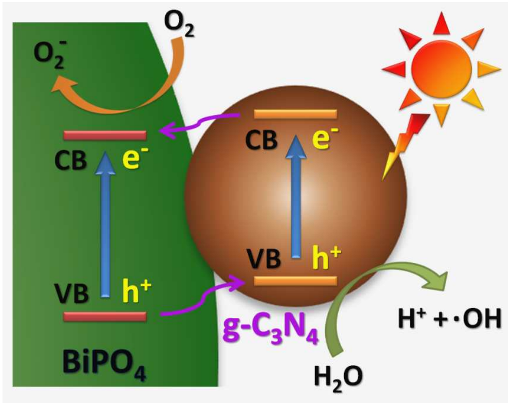

Fig.8 Schematic diagram of the separation and transport of photo-generated electron-hole pairs at the g-C_3N_4/$BiPO_4$ interface.

In conclusion, for the first time we demonstrated the synthesis of g-C_3N_4 QDs/$BiPO_4$ NCs composite photocatalysts for the advanced application of photodegradation water purification. The as-prepared g-C_3N_4 QDs has uniform and ultrathin nanostructures, which are well assembled on the surface of $BiPO_4$ NCs without the extraneous adhesive agents. Due to the potential high specific surface area and favorable heterostructures, the g-C_3N_4 QDs/$BiPO_4$ NCs composite photocatalyst exhibited significantly enhanced photocatalytic activity for the degradation of methylene orange under visible-light irradiation. The decolorization rate of can reach 92% for the g-C_3N_4 QDs/$BiPO_4$ NCs, while that of single g-C_3N_4 was only about 75%. The photocatalytic activity on the base of g-C_3N_4 QDs in g-C_3N_4 QDs/$BiPO_4$ NCs can be estimated to be 13.5 times as high as that of single g-C_3N_4. The present findings suggest that this novel g-C_3N_4 QDs/$BiPO_4$ NCs composite architecture could be used as one of promising visible light-induced photocatalysts for the degradation of organic dyes.

Acknowledgements

This research was supported by the National Natural Science Foundation of China (21173088 and 21105030), Special guidance project for the development of Guangdong high tech zone (2011B010700060), Science and technology project of Maoming (2014006) and Doctor startup project of school (513086).

Notes and references

1 (a) A. Kubacka, M. Fernandez-Garcia and G.Colon, *Chem. Rev.*, 2012, **112**, 1555-1614; (b) A. Manoj and A. Walid, *RSC Adv.*, 2013, **3**, 4130-4140; (c) Y. Tian, B. Chang, Z. Yan, B. Zhou, F. Xi and X. Dong, *RSC Adv.*, 2014, **4**, 4187-4193.

2 (a) F. Wang, D. Zhao, Z. Xu, Z. Zheng, L. Zhang and D. *J. Mater. Chem. A*, 2013, **1**, 9132-9137; (b) J. Xiong, G. Cheng, F. Qin, R. Wang, H. Sun and R. Chen, *Chem. Eng. J.*, 2013, **220**, 228-236.

3 H. Zhang, H. Huang, H. Ming, H. Li, L. Zhang, Y. Liu and Z. Kang, *J. Mater. Chem.*, 2012, **22**, 10501-10506.

4 H. Li, R. Liu, Y. Liu, H. Huang, H. Yu, H. Ming, S. Lian, S. Lee and Z. Kang, *J. Mater. Chem.*, 2012, **22**, 17470-17475.

5 L. Ge, F. Zuo, J. Liu, Q. Ma, C. Wang, D. Sun, L. Bartels and P. Feng, J. Phys. Chem. C, 2012, **116**, 13708-13714.

6 F. Xiao, J. Miao and B. Liu, *J. Am. Chem. Soc.*, 2014, *136*, 1559-1569.

7 (a) X. Wang, K. Maeda, A. Thomas, K. Takanabe, G. Xin, J.M. Carlsson, K. Domen and M. Antonietti, *Nat. Mater.*, 2009, **8**, 76-80; (b) Z. Lin and X. *Wang, Angew. Chem. Int. Ed.*, 2013, **52**, 1735-1738; (c) B. Long, J. Lin, X. Wang, *J. Mater. Chem. A,* 2014, **2**, 2942-2951.

8 (a) Y. Wang, X. Wang and M. Antonietti, *Angew. Chem. Int. Ed.*, 2011, **50**, 2-24; (b) Y. Zheng, J. Liu, J. Liang, M. Jaroniec and S. Qiao, *Energy Environ. Sci.*, 2012, **5**, 6717-6731.

9 (a) S. Yan, Z. Li and Z. Zou, *Langmuir*, 2009, **25**, 10397-10401; (b) Y. Cui, Z. Ding, P. Liu, M. Antonietti, X. Fu and X. Wang, *Phys. Chem. Chem. Phys.*, 2012, **14**, 1455-1462; (c) S.Yang, Y. Gong, J. Zhang, L. Zhan, L. Ma, Z. Fang, R. Vajtai, X. Wang and P. Ajayan, *Adv. Mater.*, 2013, **25**, 2452-2456.

10 (a) X. Wang, K. Maeda, X. Chen, K. Takanabe, K. Domen, Y. Hou, X. Fu and M. Antonietti, *J. Am. Chem. Soc.*, 2009, **131**, 1680-1681; (b) S. Yang, W. Zhou, C. Ge, X. Liu, Y. Fang and Z. Li, *RSC Adv.*, 2013, **3**, 631-5638.

11 J. Zhang, Y. Wang, J. Jin, J. Zhang, Z. Lin, F. Huang and J. Yu, *ACS Appl. Mater. Inter.*, 2013, **5**, 10317-10324.

12 W. Liu, M. Wang and C. Chen, *Chem. Eng. J.*, 2012, **209**, 386-393.

13 H. Wang, L. Zhang, Z. Chen, J. Hu, S. Li and Z. Wang, *Chem. Soc. Rev.*, 2014, **43**, 5234-5244.

14 (a) G. Jiang, C. Zhou, X. Xia, F. Yang, D. Tong, W. Yu and S. Liu, *Mater. Lett.*, 2010, **64**, 2718-2721; (b) P. Niu, L. Zhang, G. Liu, H. Cheng, *Adv. Funct. Mater.*, 2012, **224**,763-4770; (c) J. Tian, Q. Liu, C. Ge, Z. Xing, A. Asiri, A. Al-Youbi and X. Sun, *Nanoscale*, 2013, **5**, 8921-8924.

15 Y. Tang, Y. Su, N. Yang, L. Zhang and Y. Lv, *Anal. Chem.*, 2014, 86, 4528-4535.

16 C. Pan and Y. Zhu, *Environ. Sci. Technol.*, 2010, **44**, 5570-5574.

17 C. Pan and Y. Zhu, *J. Mater. Chem.*, 2011, **21**, 4235-4241.

18 (a) T. Lv, L. Pan, X. Liu and Z. Sun, *RSC Adv.*, 2012, **2**, 12706-12709; (b) C. Pan, J. Xu, Y. Wang, D. Li and Y. Zhu, *Adv. Funct. Mater.*, 2012, **22**, 1518-1524; (c) J. Xu, L. Li, C. Guo, Y. Zhang and W. Meng, *Appl. Catal. B-Environ.*, 2013, **130-131**, 285-292.

19 (a) G. Chen, M. Sun, Q. Wei, Y. Zhang, B. Zhu and B. Dua, *Chem. Soc. Rev.*, 2012, **41**, 782-796. (b) Z. Li, S. Yang, J. Zhou, D. Li, X. Zhou, C. Ge, Y. Fang, *Chem. Eng. J.* 2014, **241**, 344-351.

